Renormalisation of Global Mantle Dynamic Topography Predictions using Residual Topography Measurements for "Normal" Oceanic Crust

L. Cowie* [1, 2] **and N. Kusznir** [2]

[1] Present address: Centre for Earth Evolution and Dynamics (CEED), University of Oslo, Norway

[2] Earth, Ocean and Ecological Sciences, University of Liverpool, Liverpool, L69 3BX, United Kingdom

Corresponding Author: Leanne Cowie

Address: Centre for Earth Evolution and Dynamics (CEED), University of Oslo, P.O. Box 1028 Blindern, NO-0315 Oslo, Norway

Email: leanne.cowie.87@gmail.com

Phone: 07765673285

Abstract

We compare mantle dynamic topography predicted from mantle convection modelling with residual topography measurements for oceanic regions, where crustal basement thickness is 10.0 km or less. Measurements of residual topography, calculated by removing the isostatic effects of crustal thickness variation, bathymetry, sediments, ice and lithosphere thermal anomalies, from the observed topography, are inaccurate for continents and oceanic plateaus due to uncertainties in determining their crustal thickness and density. As a consequence, residual topography measurements for these regions are unsuitable for testing mantle dynamic topography predictions. Residual topography is more accurately determined for oceanic crust. We use global mapping of crustal basement thickness using gravity anomaly inversion to identify oceanic crust of 10.0 km thickness or less to select measured residual topography for comparison with predicted mantle dynamic topography. For these oceanic regions we compare mantle dynamic topography and residual topography and, using amplitude histogram matching and grid searches, compute the amplitude rescaling and shift which needs to be applied to predicted mantle dynamic topography to fit the observed residual topography. We examine three global compilations which use different approaches to determine mantle dynamic topography: (i) Steinberger (2007), which uses seismic topography deeper than 220 km to determine mantle density; (ii) Flament et al. (2013), which uses plate velocity and subduction history; and (iii) Steinberger et al. (2017), which uses seismic tomography, including that above 220 km, to determine shallow upper mantle densities. Our analysis shows that for the Steinberger (2007) and Flament et al. (2013) compilations, the predicted mantle dynamic topography for oceanic regions requires a rescaling of approximately x0.5 and a negative shift of approximately -500 m to match the observed residual topography. In contrast Steinberger et al. (2017), which includes shallow upper mantle densities above 220 km, requires only a small shift (+50 m) but a greater scaling of x0.375. Maps of renormalised (rescaled and shifted) mantle dynamic topography for Steinberger et al. (2017) show a close resemblance to measured residual topography.

Keywords

Mantle Dynamic Topography

Residual Topography

Oceanic crust

Gravity Inversion

1. Introduction

Large-scale variations in the Earth's surface topography originate from both changes in crustal and lithosphere thickness, lithosphere temperature structure and composition, and from convective viscous flow within the mantle (e.g. Ricard et al. (1993); Lithgow-Bertelloni and Silver (1998); Gurnis et al. (2000) and Steinberger (2016)). These two contributions to the support of the Earth's topography have been termed isostatic and mantle dynamic (Allen, 1997). Mantle dynamic topography includes both the consequences of whole-mantle thermal convection resulting in the large scale three-dimensional variations in mantle density, and smaller smaller-scale convection processes associated with mantle plume activity and subduction. The magnitude of mantle dynamic topography is related to the intensity and depth of mantle flow, whilst the wavelength is proportional to the scale and depth of the flow (Richards and Hager, 1984).

Two approaches may be used to examine mantle dynamic topography; (i) predictive forward modelling using 3D mantle convection and (ii) measurement by subtracting the isostatic component of topography from observed topography to give what is often termed residual topography. Within this paper we use the term mantle dynamic topography to refer to present day predictions and residual topography to refer to observations and measurements.

Knowledge of mantle dynamic topography is important, in particular the amplitude and what drives it. Due to its importance, attempts have been made to constrain mantle dynamic topography using observations of its geological pattern, and many authors have used the observations of residual topography to test predictive models of mantle dynamic topography (e.g. Lithgow-Bertelloni and Silver (1998); Kaban et al. (1999); Gurnis et al. (2000); Panasyuk and Hager (2000); Flament et al. (2013) and Steinberger et al. (2017)).

While at long wavelengths a global comparison of measured residual topography with predicted mantle dynamic topography shows some similarity, significant differences are observed particularly in the Pacific regions where mantle dynamic topography is substantially more positive than residual topography. Many

authors (e.g. Watkins and Conrad (2018); Steinberger et al. (2017); Hoggard et al. (2016) and Yang and Gurnis (2016)) believe that predicted mantle dynamic topography amplitudes are too great when compared to observations of residual topography. Steinberger (2016) suggests that at long wavelengths, corresponding to degree 2, the amplitude of predicted mantle dynamic topography may be twice as large as the observed residual topography. Hoggard et al. (2016) suggest that the power spectrum for predicted mantle dynamic topography at long wavelengths may be an order of magnitude greater than the observed residual topography, while at short wavelengths the opposite occurs with greater amplitudes in the residual topography compared with predicted mantle dynamic topography.

It is therefore important to better constrain the mantle dynamic topography models. Many groups have used observations of residual topography to constrain predictions of mantle dynamic topography. Watkins and Conrad (2018) developed new constraints on the amplitude of long-wavelength mantle dynamic topography by examining asymmetries in seafloor bathymetry across mid-ocean ridges. Steinberger (2016) compares predicted mantle dynamic topography, from a new model incorporating shallow upper mantle density structure, with observations of residual topography, in terms of both correlation and amplitude ratio. Yang and Gurnis (2016) investigated the relationship between free-air gravity and mantle dynamic topography as a function of wavelength and also investigated the possibility that the observed free-air gravity anomalies and the large amplitude long-wavelength mantle dynamic topography can be reconciled. They attempted to verify that at long wavelengths their predicted mantle dynamic topography is consistent with observed residual topography (from Hoggard et al. (2016)), in both pattern and amplitude. Steinberger et al. (2017) used the unclear nature of the interpretations of two large, seismically slow regions in the lower mantle beneath Africa and the Pacific oceans (and whether they are large-scale active upwellings or represent collections of regular mantle plumes) to investigate the implications of these upwellings for mantle dynamic topography. In order to do this, they compared their modelled mantle dynamic topography with a new compilation of observed residual topography.

While there is much uncertainty in the model prediction of mantle dynamic topography, there is also uncertainty in the measured residual topography particularly for the continental regions. The calculation of

96 the isostatic topography component for the continents requires knowledge of crustal thickness and density,
97 both of which are uncertain. Similar problems in determining the isostatic correction for topography exist
98 for oceanic plateaus and micro-continents in oceanic regions. Residual topography is more reliably
99 measured in oceanic regions where oceanic crust is of normal or near normal thickness.

100 In this paper we use an alternative and independent method to compare predicted mantle dynamic
101 topography with observed residual topography. In addition, we produce global maps of renormalised
102 mantle dynamic topography which provide a better fit the measured residual topography. As a strong
103 contribution to the present-day surface topographic signal arises from crustal thickness variations, we
104 restrict the comparison of predicted mantle dynamic topography with residual topography to oceanic
105 regions with normal or near normal crustal thickness where uncertainty in crustal thickness and density are
106 minimized. To achieve this, we use global mapping of crustal thickness, from gravity inversion, to identify
107 normal thickness oceanic crust and avoid oceanic plateaus and micro-continents.

108 2. Compilations of Observed Residual Topography and Predicted Mantle Dynamic
109 Topography Examined in this Study

110 We compare mantle dynamic topography with residual topography for three predictive models. These are:
111 Steinberger (2007); Flament et al. (2013); and Steinberger et al. (2017), as shown in Figure 1. We choose
112 these because they represent distinct approaches for the prediction of mantle dynamic topography.

113 The Steinberger (2007) model used a mantle convection model following the approach of Hager and
114 O'Connell (1979, 1981). Density distribution within the convection model (below 220 km) was derived from
115 seismic tomography assuming velocity anomalies are the result of temperature variations. The model
116 surface boundary condition used present-day plate velocities from NUVEL (DeMets et al., 1990). The
117 effects of the 660 and 410 km phase transitions were included in the model.

118 The Flament et al (2013) model used an approach based on subduction history similar to Ricard et al. (1993).
119 The surface boundary conditions of the mantle convection models used plate velocities for the last 200 Myr
120 derived from Seton et al. (2012) to compute the subduction input into the mantle. In order to suppress the

effect of surface traction imposed by plate velocities, the dynamic topography itself is computed with a no-slip surface boundary condition. This modelling methodology only produces the long wavelength components of mantle dynamic topography, in contrast to the approach used by Steinberger (2007) which also produces shorter wavelength components.

The Steinberger et al. (2017) model uses a methodology based on that used in Steinberger (2007) but with additional features. In particular it differs in that it includes the density anomalies derived from tomography above 220 km (as well as those below).For the comparison of predicted mantle dynamic topography and measured residual topography it is important that the residual and mantle dynamic topography models are derived in a mutually consistent manner (e.g. the oceanic lithosphere thermal correction). As a consequence, for the comparison we use the paired grids compilations of mantle dynamic and residual topography, which have been provided by Steinberger and Flament.

The Steinberger (2007) residual topography grids were prepared using an isostatic correction for ocean lithosphere cooling with oceanic ages from Mueller (1997) and an isostatic correction for continental crustal thickness variation using Crust2.0. The Steinberger (2007) residual topography (and mantle dynamic topography) grids are air loaded for both oceans and continents.

For oceanic regions the Flament et al (2013) residual topography grids were prepared using the plate cooling model of Crosby & McKenzie (2009) and a sediment correction. For continental regions a mean elevation correction was applied rather than a correction for crustal thickness variation. Consequently, the residual topography for the continents (and continental shelves) is likely to be unreliable. The oceanic values are however, more reliable and are used in this study. The Flament et al (2013) residual topography (and mantle dynamic topography) grids are water loaded for oceans and air loaded for the continents.

For the oceans the Steinberger et al. (2017) residual topography grids were based on the detailed compilation of Hoggard et al. (2016) which were made using corrections for ocean lithosphere age, sediment thickness and oceanic crustal thickness variations. For the continents, the corrections for crustal thickness variations were made using Crust2.0. The Steinberger et al. (2017) residual topography (and mantle dynamic topography) grids are air loaded for both oceans and continents.

All three compilations show positive mantle dynamic topography and residual topography in the SW Pacific (Figure 1). However, the predicted mantle dynamic topography for Steinberger (2007) and Flament et al. (2013) is much larger in amplitude and extent than the observed residual topography. For the Steinberger (2007) compilation the residual topography is positive for east Asia and eastern South America, while the corresponding mantle dynamic topography is negative. For the Flament et al. (2013) compilation a major discrepancy is seen for Eurasia and the west coast of South America where in both cases the residual topography is positive while the mantle dynamic topography is negative. We attribute these differences in the Flament et al. (2013) compilations to an inappropriate procedure used to determine their continental residual topography. In contrast we do not see such obvious discrepancies within the Steinberger et al. (2017) compilations.

3. Identification of the Global Distribution of "Normal" Thickness Oceanic Crust

The aim of this study is to compare predicted mantle dynamic topography with observed residual topography for oceanic regions where the isostatic correction for crustal thickness variation can be made more accurately. This requires the identification of oceanic crust with "normal" thickness oceanic crust, which we determine using global mapping of oceanic crustal thickness using gravity anomaly inversion as shown in Figure 2 (a).

The data used within the gravity anomaly inversion are bathymetry (Amante and Eakins, 2009), satellite derived free air gravity (Sandwell et al., 2014), three-dimensional sediment thickness (Divins, 2003; Laske and Masters, 1997) and ocean age isochrons from Müller et al. (1997). The sediment thickness, used within the gravity anomaly inversion, is a merged compilation of both the Laske and Masters (1997) and NOAA (Divins, 2003) sediment thickness data sets, in which the merged resulting sediment thickness is the larger of the two values.

The gravity anomaly inversion method is carried out in the 3D spectral domain, using the scheme of Parker (1972) to predict Moho depth and hence determine crustal basement thickness. A detailed description of the gravity anomaly inversion technique methodology is given in Chappell and Kusznir (2008), Alvey et al.

(2008), Cowie and Kusznir (2012) and Kusznir et al. (2018). A lithosphere thermal gravity anomaly correction is incorporated to account for the elevated geothermal gradient within oceanic and rifted continental margin lithosphere; failure to include the correction for the lithosphere thermal gravity anomaly can lead to predictions of Moho depth and crustal basement thickness which are substantially too great.

The gravity inversion methodology to produce crustal thickness requires a reference Moho depth to determine 3D Moho depth (Chappell and Kusznir, 2008). The reference Moho depth is the notional depth of the Moho for a region with zero topography or bathymetry, zero sediment thickness, zero long wavelength free-air gravity anomaly and zero lithosphere thermal gravity anomaly. The reference Moho depth has a global average of approximately 38 km from calibration against seismic observation, assuming a crustal basement density of 2850 kgm^{-3}, and is independent of whether the crust is oceanic or continental. Because the long wavelength components of the Earth's gravity anomaly field are controlled by deep mantle dynamic processes, which are not related to lithosphere and crustal structure, the reference Moho depth varies globally and correlates weakly with mantle dynamic topography. In this study a constant value of reference Moho depth of 38 km has been used, which assumes zero mantle dynamic topography.

The resulting global map of crustal basement thickness determined from gravity anomaly inversion is used to identify crust with thicknesses greater than that of "normal" oceanic crust, in order to eliminate and filter out the less accurate measurements of residual topography for regions of thicker crust. White et al. (1992) report that seismic refraction results show that "normal" oceanic crust averages 7.1 ±0.8 km away from anomalous regions, such as fracture zones and hotspots. The upper and lower bounds of "normal" oceanic crustal thickness range between 5.0 km and 8.5 km. When identifying regions of thick oceanic crust, sensitivities to oceanic crustal basement thickness filters with maximum values of 5.0 km, 7.0 km and 10.0 km (Figure 2 (b, c and d)) have been considered, in order to be inclusive and ensure magma poor and magma rich regions are accounted for. Whilst we show the results for these sensitivities, our preference is for the 10.0 km crustal basement thickness filter to maximise the sampling of oceanic regions.

4. Comparison of Observed Residual Topography and Predicted Mantle Dynamic Topography for "Normal" Thickness Oceanic Crust

Cross-plots of global predicted mantle dynamic topography against measured residual topography at identical locations for the Steinberger (2007), Flament et al. (2013) and Steinberger et al. (2017) compilations are shown in Figure 3 (a, e and i). Both the Steinberger (2007) and Flament et al. (2013) compilations show a highly scattered cloud of points with poor correlation between predicted mantle dynamic topography and measured residual topography. In contrast, the Steinberger et al. (2017) compilation shows a tighter cloud of points, with a more positive correlation. The global cross-plots, in Figure 3, show points that plot generally within the range -1000 m and 1000 m for both mantle dynamic topography and residual topography. The measured residual topography from the Flament et al. (2013) compilation shows a sharp cut-off at -750 m; the cause of this is explained by Flament et al. (2013) (see below also). The poor correlation of global mantle dynamic topography with residual topography shown in Figure 3 (a and e) for the Steinberger (2007) and Flament et al. (2013) compilations may be in part due to errors within the crustal thickness and density component of the determination of residual topography, particularly in continental regions.

When the crustal basement thickness filter is applied, for crust of 10.0 km thickness or less (Figure (d)), the cross-plot for the remaining regions of "normal" oceanic crust shows a tighter range for all three compilations (Figures 3 (b, f and j). As the values for thicker crust are removed, the more positive residual topography values are filtered out.

The comparison of predicted mantle dynamic topography and measured residual topography can also be made using an amplitude histogram plot as shown in Figure 3 (c, g and k). The result of applying the crustal thickness filter to produce histograms of mantle dynamic and residual topography for crust of thickness 10.0 km or less is shown in Figure 3 (d, h and i). The amplitude histograms for crust thinner than 10.0 km show that mantle dynamic topography, for all three compilations, has a larger amplitude compared with residual topography.

In the amplitude histograms of measured residual topography from Flament et al. (2013), shown in Figures 3 (g and h), there is an additional peak at approximately -750 m. These peaks are the result of how the residual topography has been calculated for the area between the continental shelf and the ocean floor (see Flament et al. (2013) for more details). This additional peak is reduced but not entirely eliminated for crust less than 10.0 km thickness.

Both the Flament et al. (2013) and the Steinberger et al. (2017) residual topography (Figure 3 (h and i)) are symmetrical about zero, whilst the peak of residual topography for Steinberger (2007) (Figure 3 (d)) is slightly negative; the cause and implication of this is unknown.

5. Renormalisation of Predicted Mantle Dynamic Topography

The aim of renormalisation is to adjust the predicted mantle dynamic topography to better fit the measured residual topography. Two methods have been used to calculate the rescaling factor and the shift required to renormalise the predicted mantle dynamic topography; these include a histogram matching method and a grid search using a L1 norm regularization method.

The histograms shown in Figures 4, 5 and 6 show the un-normalised mantle dynamic topography and associated renormalised mantle dynamic topography for the Steinberger (2007), Flament et al. (2013) and Steinberger et al. (2017) compilations. Crustal basement thickness filters of 5.0, 7.0 and 10.0 km have been used. Comparison of mantle dynamic topography and residual topography shows a similar relationship for all crustal thickness filter sensitivities. As the crustal thickness value in the filter is decreased, fewer points for comparison are selected and consequently the height of the histograms decreases

5.1. Renormalisation by Matching Histograms Amplitudes

We match the histograms of mantle dynamic and residual topography by rescaling and shifting the mantle dynamic topography. We apply a shift to the mantle topography in order to match the average mantle dynamic topography with the average observed residual topography. The shift is sensitive to the crustal basement thickness filter used when eliminating thicker than “normal” oceanic crustal regions. At lower crustal thickness filters the results may be less reliable as there are less data used to calculate the shift. For

247 the histogram matching we examine two different approaches. The first approach matches the height of
248 the histogram peaks of the rescaled mantle dynamic topography with that of the observed residual
249 topography, while the second approach matches their standard deviation.

250 In Figure 4 histograms of shifted and rescaled mantle dynamic topography are compared with those for
251 observed residual topography for the Steinberger (2007) compilations for crustal basement thickness filters
252 of 5.0, 7.0 and 10.0 km. The required shift and rescaling values to match histograms are shown on Figure 4.
253 For the Steinberger (2007) compilation a negative shift needs to be applied to the mantle dynamic
254 topography for all crustal thickness filters; for a crustal basement filter of 10.0 km the required shift is -665
255 m. The rescaling factor is x0.75 using the matched histogram peak method and x0.85 using the matched
256 standard deviations method. For both histogram matching methods the scaling factor decreases as the
257 crustal basement thickness filter decreases from 10.0 to 5.0 km. The dependency of the shift and the
258 rescale factors on crustal thickness filter settings is shown in Figure 7 for all three compilations.

259 Corresponding histograms for the Flament et al. (2013) compilation are shown in Figure 5. For a crustal
260 basement thickness filter of 10.0 km the required shift is -472 m while the rescaling factor is x0.775 and
261 x0.76 using the matched histogram peak and matched standard deviation methods respectively. The shift
262 shows a similar dependency on the crustal thickness filter to the analysis of the Steinberger (2007)
263 compilation (Figure 7). As before, decreasing the crustal thickness filter decreases the required scaling
264 factor for the matched histogram peak method. However, for the matched standard deviation method the
265 rescaling factor does not show a consistent trend with the crustal thickness filter.

266 Corresponding histograms for the Steinberger et al. (2017) compilation are shown in Figure 6. For a crustal
267 thickness filter of 10.0 km the required shift is +50 m while the rescaling factor is x0.375 using the matched
268 histogram peak method and x0.45 using the matched standard deviation method. The shift in this case is
269 positive and is also much smaller in comparison to the shifts calculated for the Steinberger (2007) and
270 Flament et al. (2013) compilations. For the Steinberger et al. (2017) compilation decreasing the crustal
271 thickness filter decreases the required scaling factor for both the matched histogram peak and standard
272 deviation methods.

5.2. Renormalisation by Grid Search using L1 Norm Regularization Method

We also determine the rescaling factor and shift to match mantle dynamic and residual topography by applying a grid search using a L1 norm regularization method (Figure 8). The L1 norm method minimizes the sum of absolute differences between the target value (residual topography in this paper) and the estimated value (mantle dynamic topography in this paper) at each identical point, and assumes that there is a correlation between these two parameters. A grid search is carried out varying the rescaling factor and shift to identify the minimum misfit. Within the grid search we are attempting to correlate a long wavelength parameter (mantle dynamic topography) with a measured parameter with both short and long wavelength components (residual topography). For obvious reasons it is inappropriate to spatially filter the residual topography.

The results of the L1 norm grid search method are shown in Figure 8 for all three compilations for crustal thickness filter sensitivities of 5.0, 7.0 and 10.0 km or less. The calculated shift of mantle dynamic topography determined using this grid search L1 norm method is approximately -800 m,-500 m and +100 m for the Steinberger (2007), Flament et al. (2013) and Steinberger et al. (2017) compilations respectively, which are similar to those calculated from the histogram matching methods. However, the re-scaling factor from the grid search L1 method is between x0.1 and x0.2 which is much less than the x0.8 from histogram matching, for both Steinberger (2007) and Flament et al. (2013). In contrast, the L1 method re-scaling factor is approximately x0.3 for Steinberger et al. (2017), which is much closer, yet still less than that calculated from the matched histograms method.

The smaller rescaling factors may be the result of a weak correlation between the predicted mantle dynamic topography and the measured residual topography, which is more apparent for the Steinberger (2007) and Flament et al. (2013) compilations . In order to test the weak correlation hypothesis, the mantle dynamic topography was set to zero and compared to the real residual topography within the grid search; the grid search yields a rescaling factor of zero. This suggests that the grid search method is not a reliable method for calculating the rescaling factor, if the correlation is weak between the predicted mantle dynamic topography and the measured residual topography.

299 Our preference is for the renormalisation rescaling factor and shift calculated from the histogram matching
300 method.

301 6. Comparison with other studies

302 We have compared our rescaling of mantle dynamic topography to fit measured residual topography with
303 other studies, in particular recent papers by Hoggard et al. (2016) and Steinberger (2016).

304 Hoggard et al. (2016) use power spectral analysis of their observed residual topography and published
305 predictive models of mantle dynamic topography in order to investigate the differences between them.
306 They show that the power spectrum of the predicted mantle dynamic topography models shows a peak at
307 long wavelengths, which decreases to zero at shorter wavelengths, whilst the power spectrum of the
308 observed residual topography has a more consistent power for all wavelengths (i.e. its spectrum is flatter).
309 In comparison with the power spectral analysis for the mantle dynamic topography, the residual
310 topography has approximately an order of magnitude less power at the longer wavelengths; however, at
311 shorter wavelengths the residual topography has significantly greater power. Our renormalisation results
312 are consistent with these long wavelength observations.

313 Steinberger (2016) presents a new mantle dynamic topography model incorporating densities shallower
314 than 220 km depth, derived from seismic tomography, which he compares with observed residual
315 topography using correlation and amplitude ratios. Various sensitivity analyses have been considered,
316 including but not limited to mantle viscosity, velocity-density scaling and surface boundary conditions. His
317 preferred model predicts a topography only slightly greater (x1.2) than residual topography, and also
318 provides an acceptable fit to the geoid. This preferred mantle dynamic topography prediction is similar in
319 amplitude to our renormalisation results for the Steinberger et al. (2017) compilation.

320 7. Renormalised Mantle Dynamic Topography

321 Figure 9 shows a comparison of the original modelled and renormalised mantle dynamic topography for
322 Steinberger (2007), Flament et al. (2013) and Steinberger et al. (2017) where the rescaling factor and shift
323 was derived from the matched heights of histogram peaks method for crustal thicknesses of 10.0 km or less

(Figures 4, 5 and 6). Renormalisation using the matched histogram standard deviations method produces maps which are not significantly different.

Both the renormalisation of mantle dynamic topography for the Steinberger (2007) and Flament et al. (2013) compilations (Figure 9 (d and e)) require a substantial negative shift (-665 m and -472 m respectively) and an amplitude reduction rescaling (x0.75 and x0.77 respectively). The renormalisation of mantle dynamic topography for the Steinberger (2017) compilation, in contrast, uses a much smaller shift (+50 m) but a more substantial rescaling factor is required (x0.375).

The renormalised mantle dynamic topography from Steinberger (2007) shows a Pacific Ocean with positive mantle dynamic topography restricted to the South West Pacific. Elsewhere in the Pacific and also in the Atlantic and Indian Oceans renormalised mantle dynamic topography is negative. Negative mantle dynamic topography is also predicted, by renormalisation, for the Americas, Africa and Eurasia. The negative renormalised mantle dynamic topography for Africa in particular suggests that the negative renormalisation shift is too great and incorrect.

The renormalised mantle dynamic topography from Flament et al. (2013) shows positive mantle dynamic topography for the Pacific and Atlantic Oceans and for South Africa. Renormalised mantle dynamic topographies for these regions are between +500 m and +1000 m. The Americas and Eurasia show negative mantle dynamic topography; for Eurasia the renormalised mantle dynamic topographies have a minimum between -1500 m and -2000 m. The Indian Ocean shows positive mantle dynamic topography in the west and negative in the east. It should be noted that the renormalisation of this and other predicted mantle dynamic topographies only use the oceanic residual topography; as a consequence the continental residual topographies of Flament et al. (2013), which are likely to be unreliable, have no impact on the renormalisation.

The renormalisation of Steinberger et al. (2017), as mentioned previously, requires a negligible offset but a more significant rescaling. As a consequence it shows a similar pattern to the original mantle dynamic topography but with lower amplitude. The renormalised mantle dynamic topography is positive in the south-west Pacific with amplitudes generally less than +500 m. Elsewhere in the east and north Pacific

values vary between ±350 m. In the Atlantic renormalised mantle dynamic topographies are negative in the west; in the Argentine Basin values are -500m and greater. The north Atlantic shows positive regions corresponding to Iceland and the Azores. Elsewhere in the eastern and south Atlantic there are regions of low amplitude negative and positive renormalised mantle dynamic topography (< ±500 m); similarly, in the Indian Ocean. South and east Africa show a positive renormalised mantle dynamic topography with values in north-east Africa exceeding +500 m. Renormalised mantle dynamic topographies for Eurasia are generally negative with values down to -500 m.

The original and renormalised mantle dynamic topographies for Steinberger et al. (2017) differ from those of Steinberger (2007) and Flament et al. (2013) in that they contain shorter wavelength components. This arises from the inclusion of seismic tomography data for depths of less than 220 km to provide lithosphere density information for the mantle convection modelling. It is conspicuous that while histogram matching of mantle dynamic and residual topography for the Steinberger (2007) and Flament et al. (2013) compilations required a substantial shift of -500 m or more, the Steinberger et al. (2017) compilation does not. This zero offset for Steinberger et al. (2017) is confirmed by the grid search comparison of mantle dynamic and residual topography (Figure 8). We attribute this zero offset for the Steinberger et al. (2017) compilation to the inclusion of seismic tomography information above 220 km depth in the mantle convection prediction of mantle dynamic topography.

The renormalised mantle dynamic topography for Steinberger et al. (2017) is similar to the mantle dynamic topography model which includes the effect of lateral viscosity variations above 220 km from Osei Tutu et al. (2018) (illustrated in Figure 1 (c) of Steinberger et al. (2017)). This may suggest that the amplitude reduction rescaling in our renormalisation, based on oceanic comparisons, arises because lower upper mantle viscosity in oceanic regions reduces surface coupling of mantle convection mantle dynamic forces. The more complete lithosphere density structure within the mantle dynamic topography modelling and the inclusion of both long and short wavelengths makes the Steinberger et al. (2017) compilations our preference for the renormalisation results.

The comparison of modelled mantle dynamic and measured residual topographies, and the shift and rescaling to give renormalised mantle dynamic topography, has been carried out for oceanic crust of normal or near normal thickness with thicknesses less than or equal to 10.0 km. Due to the large errors and uncertainties in determining residual topography for the continents we do not believe that it is possible to carry out a meaningful comparison or recalibration for the continents. In Figure 10 we compare the observed residual topography with the renormalised topography for Steinberger et al. (2017) for crust less than or equal to 10 km thick. An important question that remains is whether the renormalisation derived for oceans can be applied to continental regions.

8. Summary

We have compared the modelled mantle dynamic topography predictions of Steinberger (2007), Flament et al. (2013) and Steinberger et al. (2017) with their associated measured residual topography. Due to the large errors and unreliability of measured residual topography in continental regions, oceanic plateaus and micro-continents, we restrict our comparisons to oceanic regions with crustal thickness less than 10.0 km, which corresponds to oceanic crust with normal (or near normal) crustal thickness where crustal thickness isostatic corrections may be made with more confidence. The amplitude rescaling and shift of predicted mantle dynamic topography to correspond to measured residual topography in oceanic regions has been examined using histogram matching and grid search methods. While the mantle dynamic topography predictions of Steinberger (2007) and Flament et al. (2013) were made using very different approaches (the former using seismic tomography and the latter subduction history to condition mantle convection models), the oceanic comparison with measured residual topography in both cases suggests that predicted mantle dynamic topography is too positive and also too large. Shifts of -665 m and -470 m and rescaling by x0.75 and x0.77 of predicted mantle dynamic topography are required for the Steinberger (2007) and Flament et al. (2013) compilations respectively. In contrast, the compilation of Steinberger et al. (2017), which included density heterogeneities above 220 km derived from seismic tomography in the prediction of mantle dynamic tomography, requires no significant shift but a larger rescaling, by x0.375.

Our conclusion is that the predicted mantle dynamic topography in oceanic regions is too large and needs to be rescaled by approximately x0.35 (between x0.3 and x0.4). At long wavelengths our analysis is consistent with the results of Hoggard et al. (2016) who use a different approach. They show that at long wavelengths predicted mantle dynamic topography is between x2 and x10 larger than observed residual topography (while at shorter wavelengths, they show that residual topography has greater amplitude than the predicted dynamic topography from models that exclude uppermost mantle density anomalies). The required rescaling of oceanic predicted mantle dynamic topography is consistent with the suggestion made by Steinberger et al. (2017) that mantle convection mantle dynamic forces are poorly coupled to the surface because of sub-lithosphere low viscosity structure.

We show that the renormalised (rescaled) predicted mantle dynamic topography from Steinberger et al. (2017) shows good agreement with the observed residual topography for the Pacific, Atlantic and Indian Ocean. As the renormalisation can only be calibrated for oceanic regions, it is uncertain whether the same rescaling of predicted mantle dynamic topography can be applied to the continents.

Acknowledgements

LC was funded by the MM3 industry consortium. We thank Fergus Cowie for his work in preparing the data and running the initial analysis. We thank Nico Flament and Bernhard Steinberger for providing the data compilations used within this paper and for very useful discussions prior to submission. We also thank the editor Rebecca Bendick and the two reviewers, Mike Gurnis and Bernhard Steinberger for their useful comments.

Figure Captions:

Figure 1: Comparison of measured residual topography and model predicted mantle dynamic topography for the (a & d) Steinberger (2007), (b & e) Flament et al. (2013) and (c & f) Steinberger et al. (2017) compilations. **Figure 2:** (a) Global crustal basement thickness calculated from our gravity anomaly inversion. (b) Areas with crustal thickness of 5.0 km or less; (c) 7.0 km or less; (d) 10.0 km or less.

Figure 3: Comparison of the relationship between the observed residual topography and predicted mantle dynamic topography for the Steinberger (2007), Flament (2013) and Steinberger et al. (2017) compilations. Cross-plots showing the relationship between measured residual topography and predicted mantle dynamic topography (a, e & i) for all crustal basement thicknesses, and (b, f & j) for crustal thicknesses of 10 km or less. Histogram showing the relationship between measured residual topography and predicted mantle dynamic topography (c, g & k) for all crustal basement thicknesses, and (d, h & i) for crustal thicknesses of 10 km or less.

Figure 4: Histograms showing the un-normalised and renormalised relationships between measured residual topography and predicted mantle dynamic topography for the Steinberger (2007) compilation. (a, b & c) Histograms showing the un-normalised relationship between measured residual topography and predicted mantle dynamic topography filtered for crustal thickness less or equal to 5, 7 and 10 km. (d, e & f) Histograms showing residual topography and re-normalised mantle dynamic topography using the histogram matched heights method for crustal thickness less or equal to 5, 7 and 10 km. (g, h & i) Histograms showing residual topography and re-normalised mantle dynamic topography using the histogram matched standard deviations method for crustal thickness less or equal to 5, 7 and 10 km.

Figure 5: Histograms showing the un-normalised and renormalised relationships between measured residual topography and predicted mantle dynamic topography, and sensitivity to crustal thickness filter, for the Flament et al. (2013) compilation. Explanation of (a - i) similar to Figure 4. **Figure 6:** Histograms showing the un-normalised and renormalised relationships between measured residual topography and

predicted mantle dynamic topography, and crustal thickness filter, for the Steinberger et al (2017) compilation. Explanation of (a - i) similar to Figure 4.

Figure 7: (a) Sensitivity of the maximum crustal thickness filter to the calculated shift and (b) rescaling factor for the renormalisation of predicted mantle dynamic topography from the Steinberger (2007), Flament et al. (2013) and Steinberger et al. (2017) compilations. Within (b) the solid lines represent the matched peak (MP) method, whilst the dashed lines represent the standard deviation (SD) method.

Figure 8: Grid search of shift and scaling factor parameter space showing L1 norm misfit between renormalized predicted dynamic topography and observed residual topography for the Steinberger (2007), Flament et al (2013) and Steinberger et al. (2017) compilations, and sensitivity to crustal thickness filters of 5, 7 and 10 km.

Figure 9: Comparison of model predicted mantle dynamic topography and renormalised mantle dynamic topography for the (a & d) Steinberger (2007), (b & e) Flament et al. (2013) and (c & f) Steinberger et al. (2017) compilations.

Figure 10: Comparison of the (a) observed residual topography; (b) renormalised mantle dynamic topography for crust less than 10 km thick, for the Steinberger et al. (2017) compilation.

References:

Allen, P. A., 1997, Earth Surface Processes, Hoboken, John Wiley & Sons, 404 p.:

Alvey, A., Gaina, C., Kusznir, N. J., and Torsvik, T. H., 2008, Integrated crustal thickness mapping and plate reconstructions for the high Arctic: Earth and Planetary Science Letters, v. 274, no. 3-4, p. 310-321.

Amante, C., and Eakins, B. W., 2009, ETOPO1 1 Arc-Minute Global Relief Model: Procedures, Data Sources and Analysis: NOAA Technical Memorandum NESDIS NGDC-24, p. 19.

Chappell, A. R., and Kusznir, N. J., 2008, Three-dimensional gravity inversion for Moho depth at rifted continental margins incorporating a lithosphere thermal gravity anomaly correction: Geophysical Journal International, v. 174, no. 1, p. 1-13.

Cowie, L., and Kusznir, N., 2012, Mapping crustal thickness and oceanic lithosphere distribution in the Eastern Mediterranean using gravity inversion: Petroleum Geoscience, v. 18, no. 4, p. 373-380.

Crosby, A. G., and McKenzie, D., 2009, An analysis of young ocean depth, gravity and global residual topography: Geophysical Journal International, v. 178, no. 3, p. 1198-1219.

DeMets, C., Gordon, R. G., Argus, D. F., and Stein, S., 1990, Current plate motions: Geophysical Journal International, v. 101, no. 2, p. 425-478.

Divins, D. L., 2003, Total Sediment Thickness of the World's Oceans & Marginal Seas: NOAA National Geophysical Data Center.

Flament, N., Gurnis, M., and Müller, R. D., 2013, A review of observations and models of dynamic topography: Lithosphere, v. 5, no. 2, p. 189-210.

Gurnis, M., Mitrovica, J. X., Ritsema, J., and Heijst, H. J. v., 2000, Constraining mantle density structure using geological evidence of surface uplift rates: The case of the African Superplume: Geochemistry, Geophysics, Geosystems, v. 1, no. 7.

Hager, B. H., and O'Connell, R. J., 1979, Kinematic models of large ‐ scale flow in the Earth's mantle: Journal of Geophysical Research: Solid Earth, v. 84, no. B3, p. 1031-1048.

-, 1981, A simple global model of plate dynamics and mantle convection: Journal of Geophysical Research: Solid Earth, v. 86, no. B6, p. 4843-4867.

Hoggard, M. J., White, N., and Al-Attar, D., 2016, Global dynamic topography observations reveal limited influence of large-scale mantle flow: Nature Geosci, v. 9, no. 6, p. 456-463.

Kaban, M. K., Schwintzer, P., and Tikhotsky, S. A., 1999, A global isostatic gravity model of the Earth: Geophysical Journal International, v. 136, no. 3, p. 519-536.

Kusznir, N. J., Roberts, A. M., and Alvey, A. D., 2018, Crustal structure of the conjugate Equatorial Atlantic Margins, derived by gravity anomaly inversion: Geological Society, London, Special Publications, v. 476.

Laske, G., and Masters, G., 1997, A Global Digital Map of Sediment Thickness, EOS Trans: AGU, v. 78, no. F483.

Lithgow-Bertelloni, C., and Silver, P. G., 1998, Dynamic topography, plate driving forces and the African superswell: Nature, v. 395, no. 6699, p. 269 - 272.

Müller, R. D., Roest, W. R., Royer, J.-Y., Gahagan, L. M., and Sclater, J. G., 1997, Digital isochrons of the world's ocean floor: Journal of Geophysical Research, v. 102, no. B2, p. 3211-3214.

Osei Tutu, A., Steinberger, B., Sobolev, S. V., Rogozhina, I., and Popov, A. A., 2018, Effects of upper mantle heterogeneities on the lithospheric stress field and dynamic topography: Solid Earth, v. 9, no. 3, p. 649-668.

Panasyuk, S. V., and Hager, B. H., 2000, Models of isostatic and dynamic topography, geoid anomalies, and their uncertainties: Journal of Geophysical Research: Solid Earth, v. 105, no. B12, p. 28199-28209.

Parker, R. L., 1972, The Rapid Calculation of Potential Anomalies: Geophysical Journal of the Royal Astronomical Society, v. 31, no. 4, p. 447-455.

Ricard, Y., Richards, M., Lithgow ‐ Bertelloni, C., and Le Stunff, Y., 1993, A geodynamic model of mantle density heterogeneity: Journal of Geophysical Research: Solid Earth, v. 98, no. B12, p. 21895-21909.

509 Richards, M. A., and Hager, B. H., 1984, Geoid anomalies in a dynamic Earth: Journal of Geophysical
510 Research: Solid Earth, v. 89, no. B7, p. 5987-6002.
511 Sandwell, D. T., Müller, R. D., Smith, W. H. F., Garcia, E., and Francis, R., 2014, New global marine gravity
512 model from CryoSat-2 and Jason-1 reveals buried tectonic structure: Science, v. 346, no. 6205, p.
513 65.
514 Seton, M., Müller, R. D., Zahirovic, S., Gaina, C., Torsvik, T., Shephard, G., Talsma, A., Gurnis, M., Turner, M.,
515 Maus, S., and Chandler, M., 2012, Global continental and ocean basin reconstructions since 200Ma:
516 Earth-Science Reviews, v. 113, no. 3, p. 212-270.
517 Steinberger, B., 2007, Effects of latent heat release at phase boundaries on flow in the Earth's mantle,
518 phase boundary topography and dynamic topography at the Earth's surface: Physics of the Earth
519 and Planetary Interiors, v. 164, no. 1–2, p. 2-20.
520 -, 2016, Topography caused by mantle density variations: observation-based estimates and models derived
521 from tomography and lithosphere thickness: Geophysical Journal International, v. 205, no. 1, p.
522 604-621.
523 Steinberger, B., Conrad, C. P., Tutu, A. O., and Hoggard, M. J., 2017, On the amplitude of dynamic
524 topography at spherical harmonic degree two: Tectonophysics.
525 Watkins, C. E., and Conrad, C. P., 2018, Constraints on dynamic topography from asymmetric subsidence of
526 the mid-ocean ridges: Earth and Planetary Science Letters, v. 484, p. 264-275.
527 White, R. S., McKenzie, D., and O'Nions, R. K., 1992, Oceanic Crustal Thickness From Seismic Measurements
528 and Rare Earth Element Inversions: Journal of Geophysical Research, v. 97, no. B13, p. 19683-
529 19715.
530 Yang, T., and Gurnis, M., 2016, Dynamic topography, gravity and the role of lateral viscosity variations from
531 inversion of global mantle flow: Geophysical Journal International, v. 207, no. 2, p. 1186-1202.

532

Figure 1

Cowie & Kusznir, 2018

Using grids from Steinberger (2007)

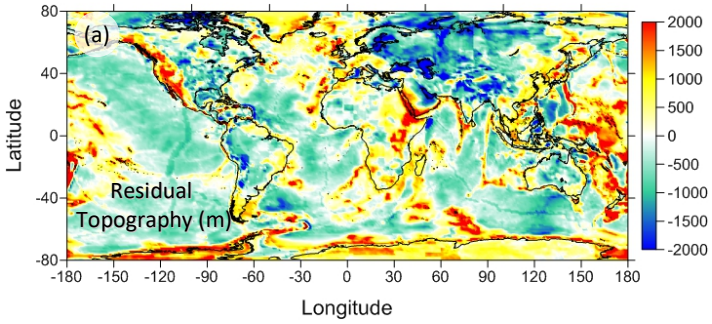

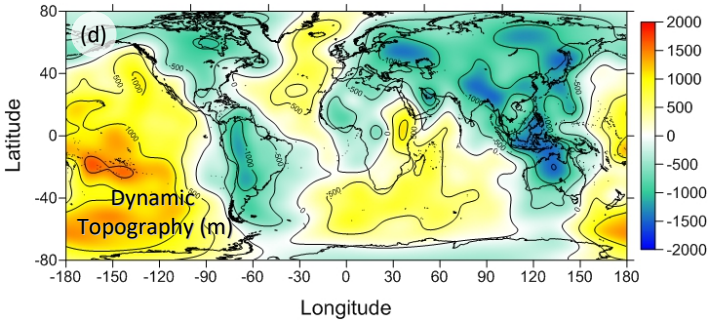

Using grids from Flament et al. (2013)

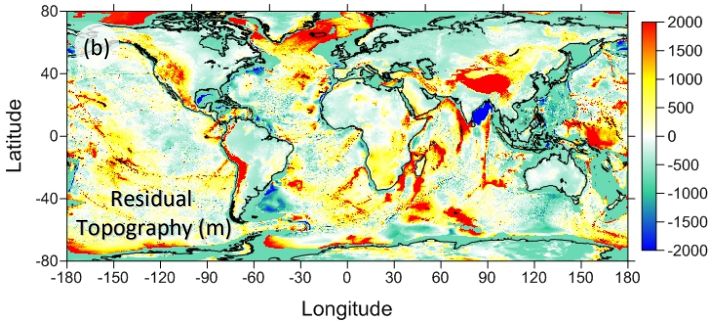

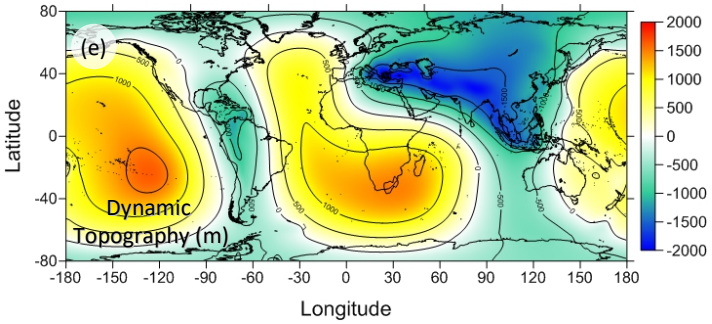

Using grids from Steinberger et al. (2017)

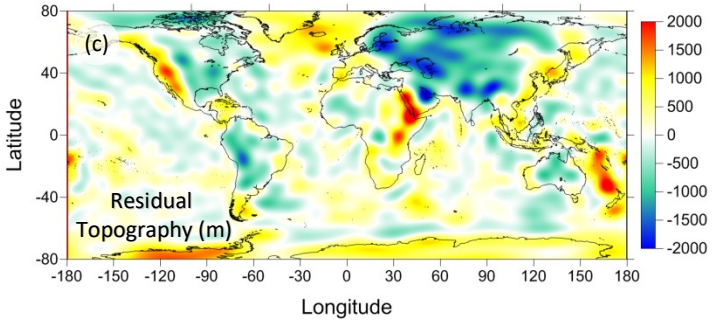

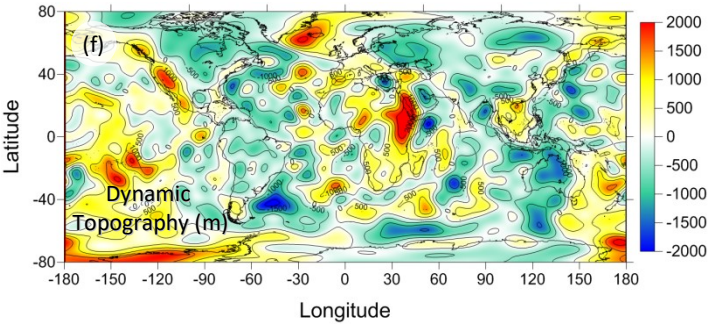

Figure 2

Cowie & Kusznir, 2018

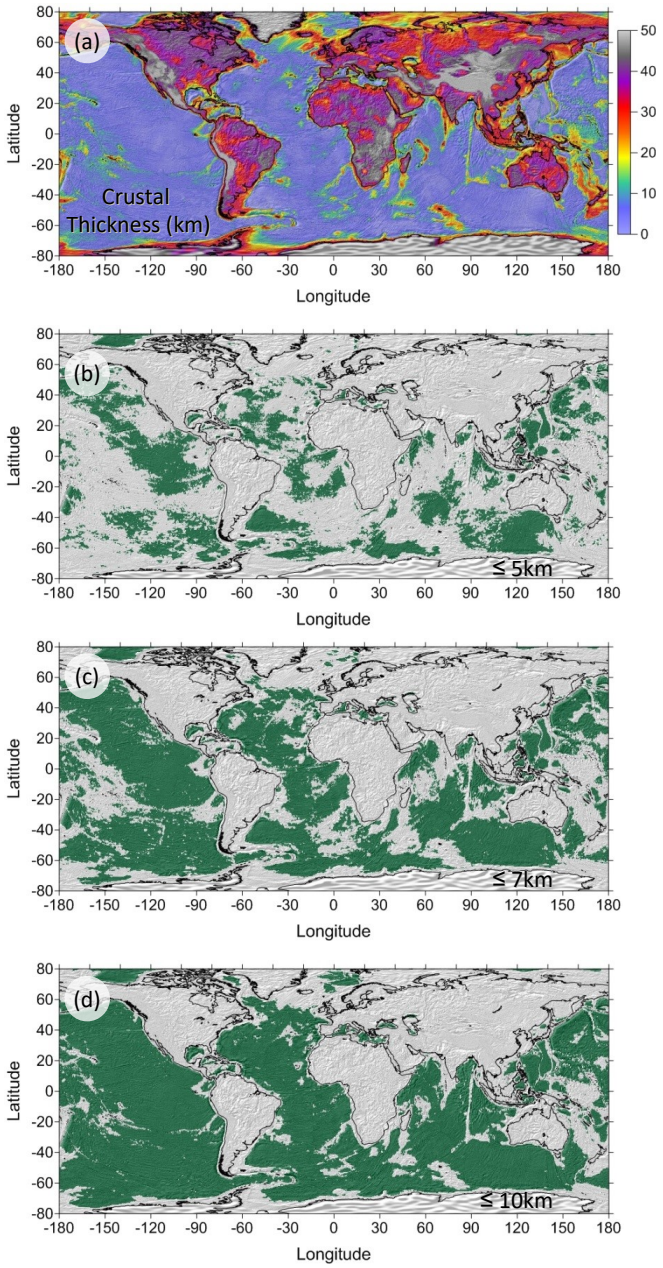

Figure 3

Cowie & Kusznir, 2018

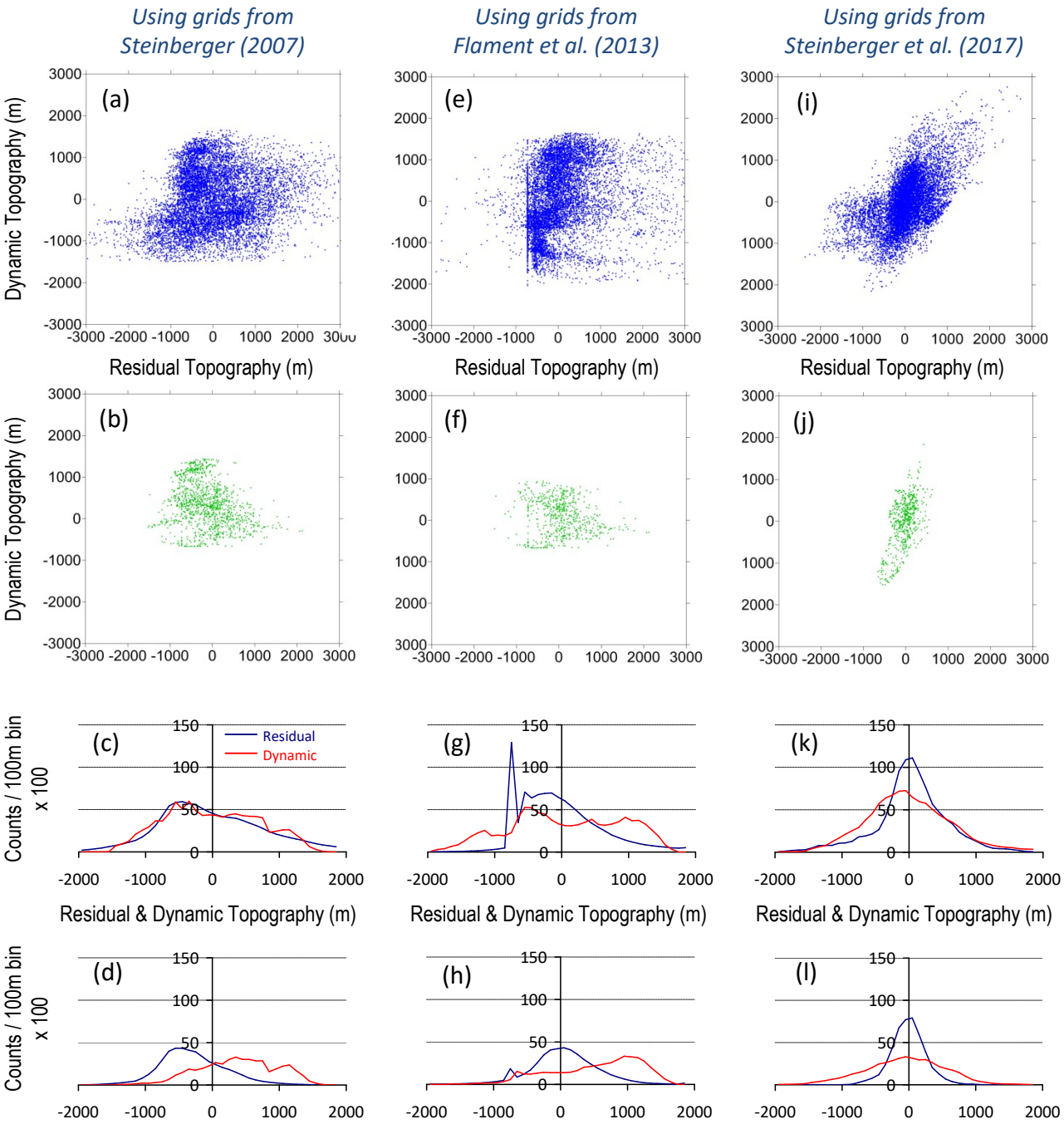

Figure 4

Cowie & Kusznir, 2018

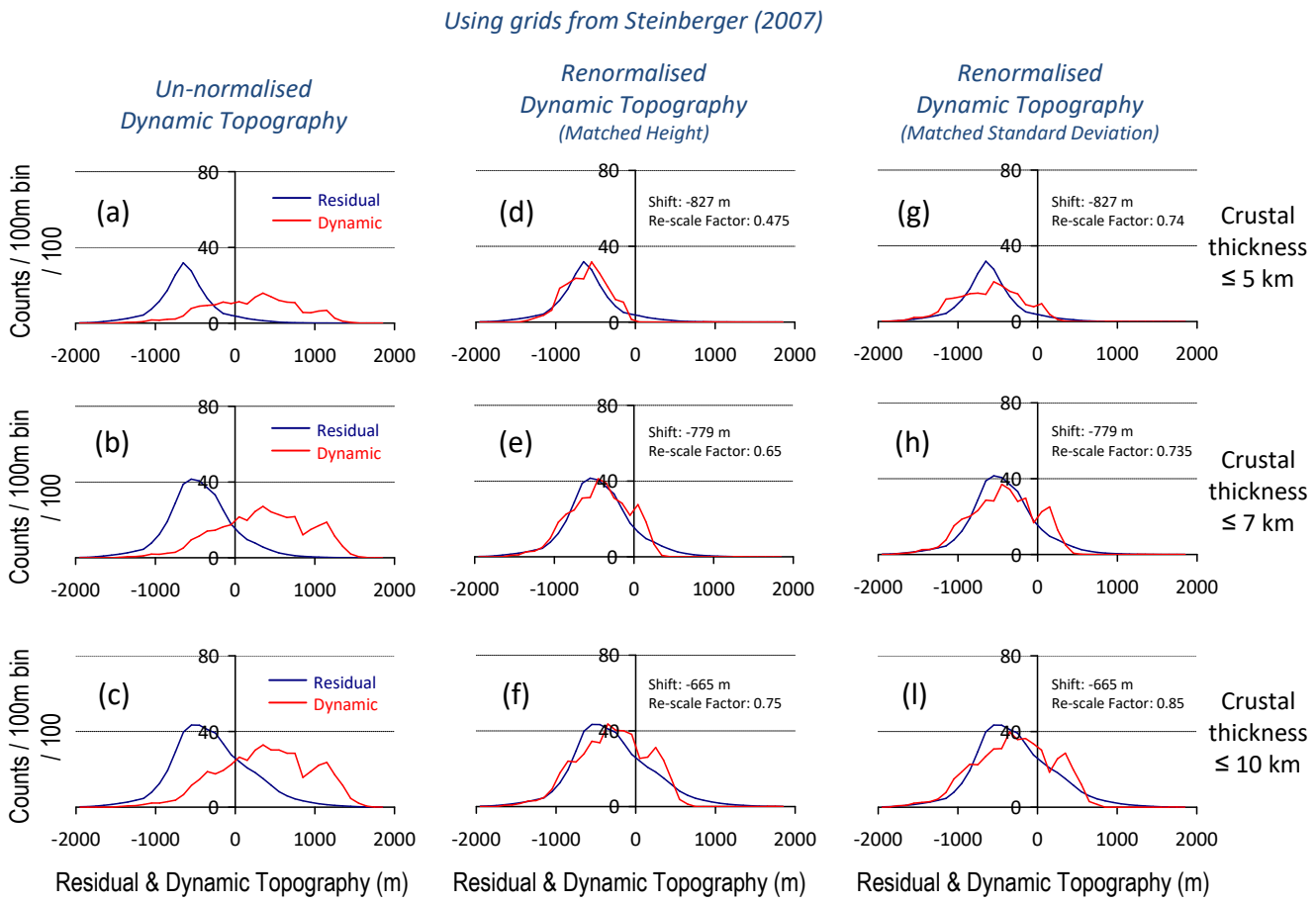

Figure 5

Cowie & Kusznir, 2018

Using grids from Flament et al. (2013)

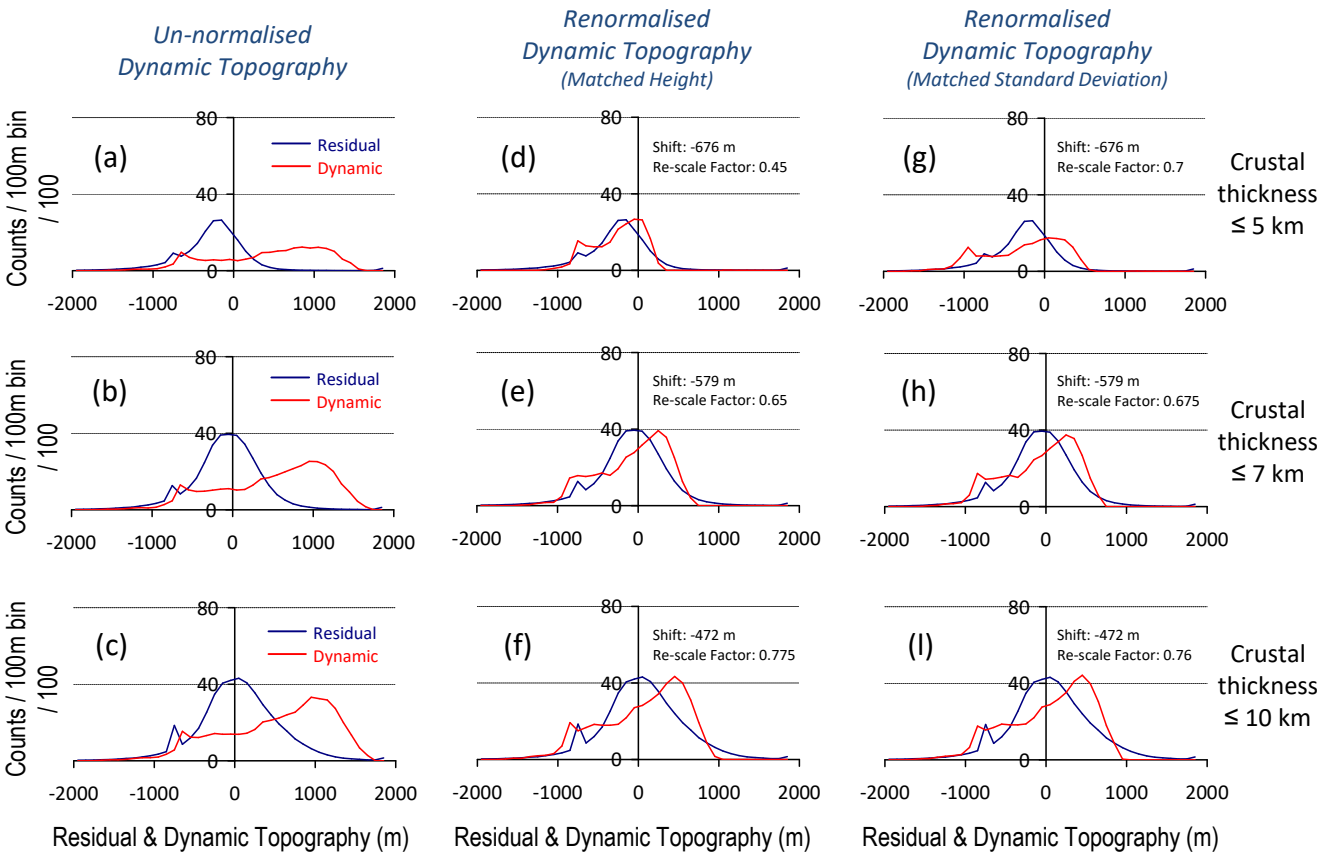

Figure 6

Cowie & Kusznir, 2018

Using grids from Steinberger et al. (2017)

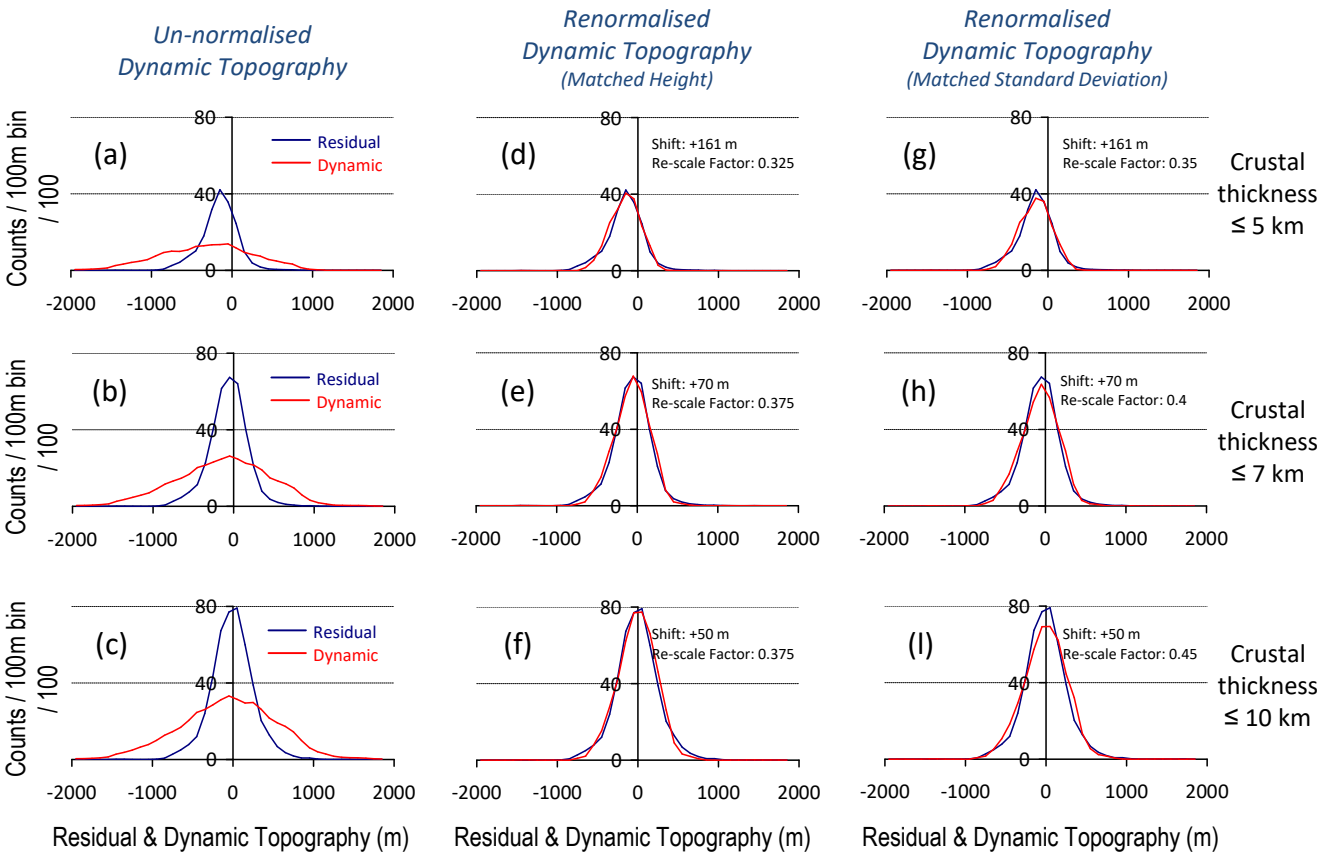

Figure 7

Cowie & Kusznir, 2018

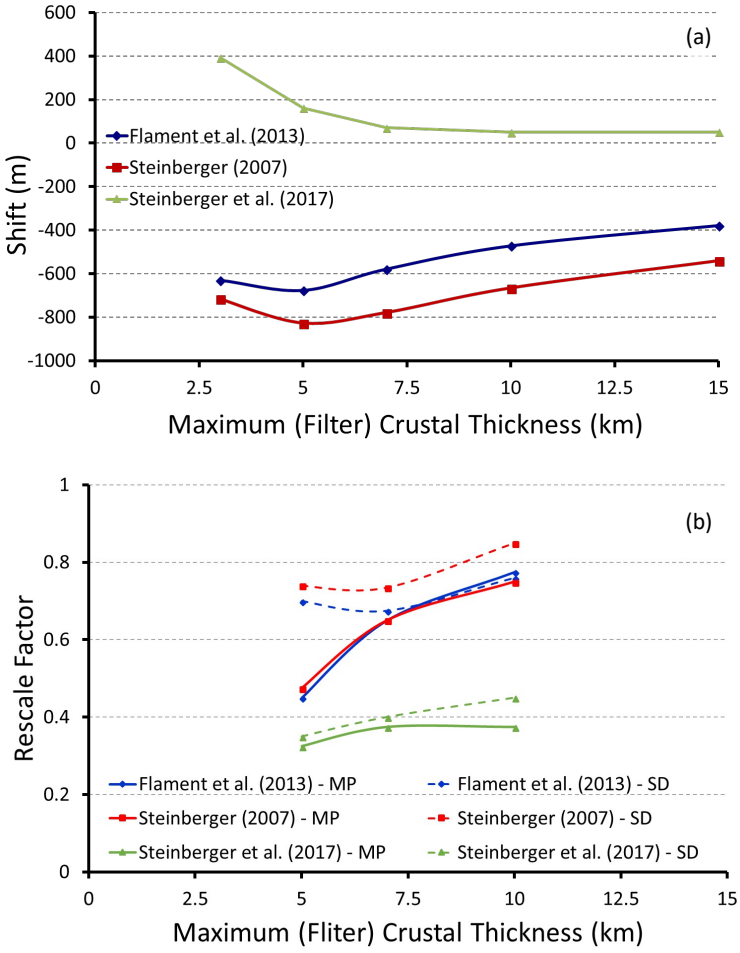

Figure 8

Cowie & Kusznir, 2018

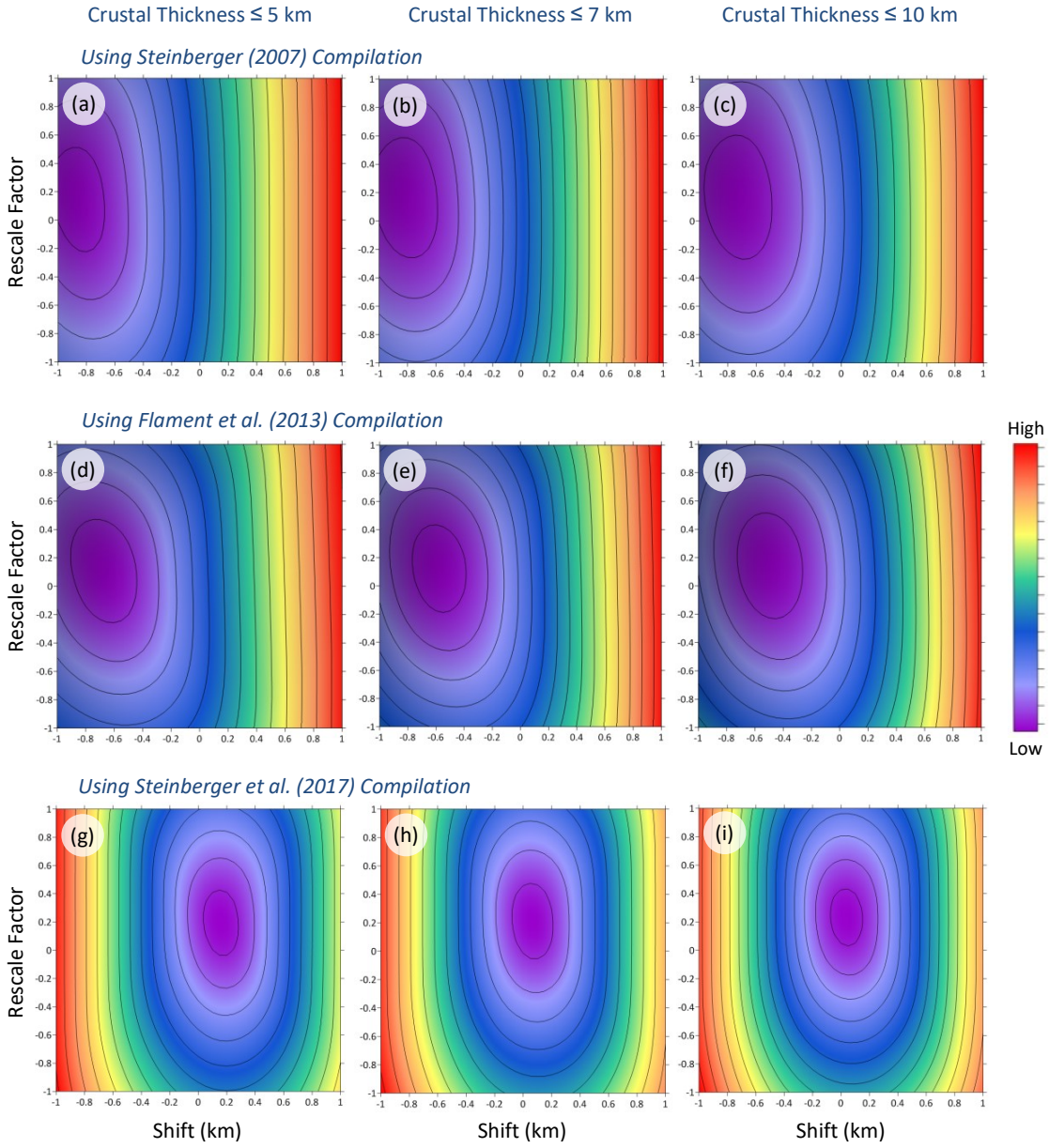

Figure 9

Cowie & Kusznir, 2018

Using grids from Steinberger (2007)

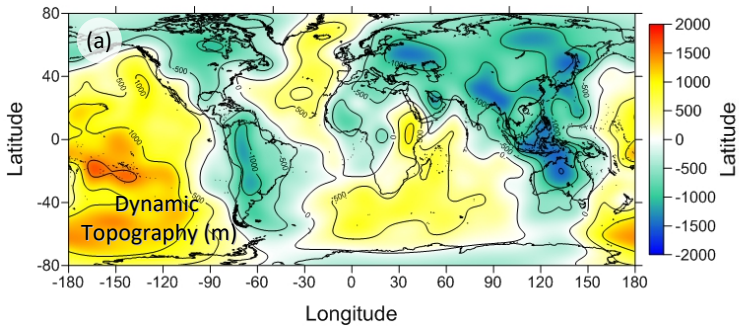

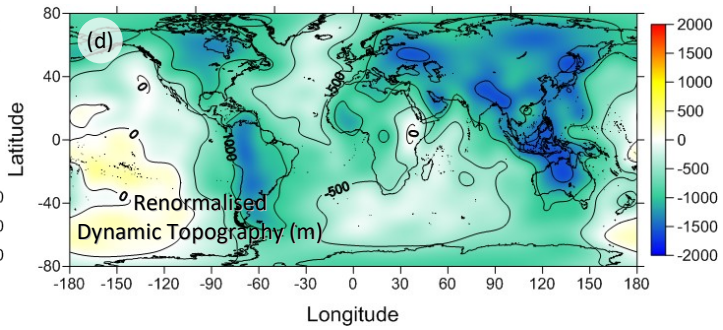

Using grids from Flament et al. (2013)

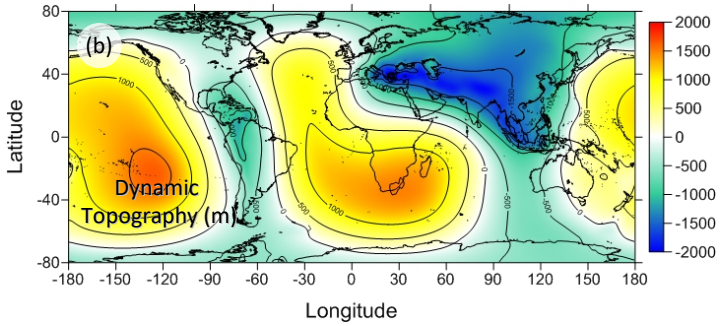

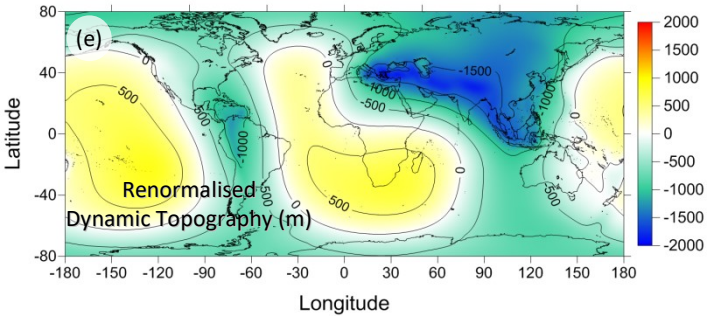

Using grids from Steinberger et al. (2017)

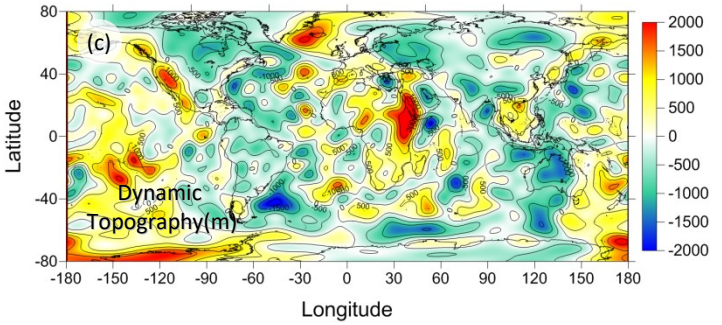

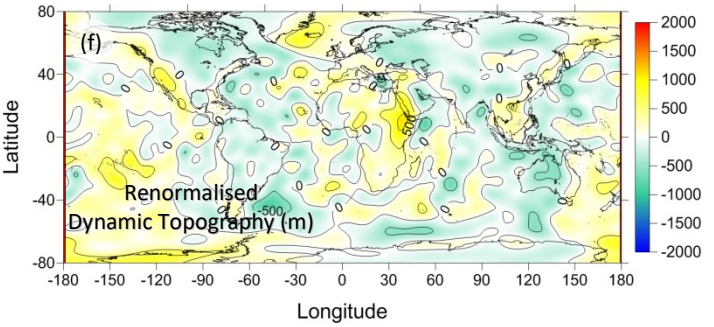

Figure 10

Cowie & Kusznir, 2018

Using grids from Steinberger (2017)